Facile Preparation of PtNPs/BSA-RGO Nanostructure for Non-Enzymatic Glucose Electrochemical Sensing

Feng Wu[1,], Qingji Xie[2], Xin Yang[1], Ouyang Yuejun[1], Yangjian Hu[1]*

[1] College of Chemistry and Material Engineering, Huaihua University, Huaihua, Hunan 418008, China
[2] Key Laboratory of Chemical Biology and Traditional Chinese Medicine Research (Ministry of Education), College of Chemistry and Chemical Engineering, Hunan Normal University, Changsha 410081, China
[*]E-mail: wufeng04303@126.com

A non-enzymatic glucose electrochemical sensing was constructed by platinum/bovine serum-reduced graphene (PtNPs/BSA-RGO) nanoconstructure modified glassy carbon electrode (GCE). The BSA-RGO composite was firstly synthesized using a hydrothermal synthesis method with BSA acted as the reductant and stabilizing reagent. Nanostructure Pt was reduced onto the BSA-RGO composites modified GCE with the formic acid reduction at room temperature. The BSA-RGO composites were characteried by Fourier transform infrared spectroscopy (FTIR), Scanning electron microscopy (SEM) X-ray diffraction (XRD) and electrochemistry techniques, and the amperometric method was used to evaluate the electrocatalytic activity towards glucose in neutral media. Under optimal conditions, the PtNPs/BSA-RGO/GCE displays a linear range from 20 µM to 7.5 mM with a sensitivity of 3.62 mA mM^{-1} cm^{-2} ($r = 0.9972$), and a detection limit of 2.0 Mm (N/S=3) which lower than many non-enzymatic electrochemical glucose sensors. The modified electrode was applied to the determination of glucose in serum sample showed a satisfactory result, indicating it was promising for the development of a novel non-enzymatic electrochemical glucose sensor.

1. INTRODUCTION

Glucose detection is very important in a variety of fields [1]. In clinical medicine, monitoring of blood glucose levels was vital for controlling the diabetes and mellitus disease [2]. As a result, the glucose sensors with higher sensitivity, better selectivity, good stability, fast response, and low cost have driven tremendous research efforts for decades [3, 4]. Although several promising methodologies including optical [5-7] and acoustic [8] technologies have been explored for glucose detection, electrochemical methods recognized as the most effective detection tool [9]. The electrochemical

glucose sensors can be categorized into non-enzymatic sensing and the enzymatic sensing [10]. The enzymatic sensing have showing good selectivity and high sensitivity [11], however, the lack of stability of the enzymatic sensors is the most serious problem [12-14]. In order to solve this problem, many non-enzyme electrochemical sensors have applied to detect glucose, especially using non-enzymatic amperometric glucose sensors. Noble metals such as Ag [15], Au [16-19], Pd [20], Pt [21, 22], Au/Pt [23], PtNi and metal oxides [24] such as CuO_x [25]and MnO_2 [26] were usually chosen to develop non-enzymatic sensors in recently years, and the Pt-based material have been used the most popular material due to its high catalytic activity even exposure in strong acid or alkaline [4]. However, Pt based material are easily poisoned by the Cl^{-1} ions in solution and adsorbed intermediates during the oxidation process [27, 28]. Recently, nanostructured Pt [23, 29], biometallic/polymetallic Pt-based material [30, 31] and nanosized Pt loading on carbon material [21, 27] were applied to overcoming influence of the chloride ions. Therefore, much effort has been put into the design of Pt-based nanomaterial to improve the performance of non-enzymatic electrochemical glucose sensors.

Being large surface areas, high electrical intriguing and chemical inertness, reduced graphene oxide (RGO) consisting of a single atomic layer of conjugated sp^2 carbon atoms has applied for a new type of supporting substrates recently [32-35]. However, RGO is easy tends to aggregate due to π-π stacking interactions. Chemical modified RGO have necessary to improve its stability and introduce special functionalities. Various methods have been developed to prepare the functional RGO, including chemical, thermal, and electro/photochemical reduction. Recently, many efforts have been made to develop metal nanoparticles/RGO nanocomposites for glucose sensing [10, 17, 18, 20, 36-38]. Liu [39] reported an environmentally friendly reduction/decoration strategy to produce functional RGO with pH-dependent solubility, and constructed a platforms toward the efficient assembly of nanoparticles with diverse sizes, shapes, compositions, and surface properties. Song [23] developed an ultrasensitive and reliable non-enzymatic electrochemical glucose sensor, which is based on mesoporous Au/Pt nanodendrites prepared by a facile route. Li [40] reported an facile electrochemical fabrication of NiO/PtNPs/electrochemically reduced graphene oxide ternary composite modified electrode for non-enzymatic electrochemical glucose sensor.

In this paper, we have firstly synthesized BSA-RGO composites with BSA acts as the reductant and the stability. The PtNPs supported on BSA-RGO modified electrode have been prepared using an in situ reduction process with formic acid as the reductant at room temperature. The PtNPs/BSA-RGO /GCE was applied for non-enzymatic electrochemical glucose sensor, and performed a broad concentration range from 20 μM to 7.5 mM with a sensitivity of 3.69 mA mM^{-1} cm^{-2} for glucose detection, the LOD was lower than many non-enzymatic electrochemical glucose sensors. This result indicating it was promising for the development of a novel non-enzymatic electrochemical glucose sensor.

2. EXPERIMENTAL SECTION

2.1 Chemical reagents and apparatus

Chloroplatinic acid ($H_2PtCl_6 \cdot 6H_2O$), formic acid, DA, UA and BSA were purchased from Sigma-Aldrich. AA and glucose were purchased from Sinopharm Chemical Reagent Co. Ltd. They

were all used as received as received. 0.1 M phosphate buffer solution (PBS, pH 7.0) was prepared using Na_2HPO_4 and NaH_2PO_4. All other chemicals were of analytical grade and used as received. Double distilled water was used throughout.

The electrochemical measurements were carried out with a CHI 660C electrochemical workstation (Shanghai Chenhua Co., China). A three-electrode electrochemical cell was used. The reference electrode was a KCl-saturated calomel electrode. A graphite rod was used as the auxiliary electrode and the working electrode was a disk GCE (Φ=3 mm) or its modified electrode. FTIR spectra was collected on a Nicolet Nexus 670 FTIR spectrophotometer equipped with a DTGS KBr detector in the region of 4000-400 cm^{-1}, and 40 scans with 4 cm^{-1} resolution for each were averaged. Raman spectra were collected on a laser Raman spectrophotometer (DXR) at a laser excitation wavelength of 532 nm. The surface morphology was characterized by the scanning electron microscopy (SEM, ZEISS-SIGMA HD).

2.2 Preparation of BSA-RGO composites

Graphene oxide (GO) was synthesized from natural graphite powders by a modified Hummers method. To obtain the modified electrode, the BSA-RGO composite was prepared as follows. 500 mg BSA was added into 40 mL 0.5 mg mL^{-1} GO solution, and sonicated for 10 min. The pH of the mixture was rapidly raised to around 12 by addition of 1.0 M NaOH. The mixture solution was sealed in a hydrothermal reactor, and being heated at 90 ^{0}C for 24 hour in a furnace. The products were centrifuged at 9560 g for several times to ensure the successful removal of free unbound BSA, the resulting black suspensions was redispersed in double distilled water, dialysised for two days, and freeze-drying.

2.3 Fabrication of the Pt/BSA-RGO/GCE sensor

After the GCE was polished with 1.0 μm and then 0.05 μm alumina slurry to obtain a mirror-like finished, 6.0 μL of 1 mg mL^{-1} BSA-RGO suspension was dropped onto the GCE and dried at room temperature, water-rinsed and dried by N_2 flow. Then, the BSA-RGO/GCE was immersed into a solution containing 1.0 mM $H_2PtCl_6 \cdot 6H_2O$ and 1 M HCOOH, after 12 h reaction, the Pt/BSA-RGO/GCE was prepared and dried by N_2 flow, which would be kept at 4 ^{0}C in refrigerator before use.

3. RESULTS AND DISCUSSION

3.1 Characterization of the materials

Figure. 1A shows the FTIR spectra of GO, BSA-RGO and BSA composites. For GO, the bands at 1093, 1373 and 1620 cm^{-1} are assigned to the C-OH stretching of COOH groups, the O-H deformation band of the C-OH groups and the epoxy groups and the skeletal ring vibrational band, respectively. For BSA-RGO, the bands at 1065, 1400 and 1740 cm^{-1} were evidently decrease or disappear in intensity comparing to the pure BSA (curve c), suggesting the oxygen-containing

functional groups of GO were removed to a large degree after the BSA reduction in alkaline conditions.

The Raman spectra of GO and BSA-RGO composite were shown in Figure. 1B. Two prominent scattering peaks located at 1310 and 1590 cm^{-1} can be assigned to the E_{2g} phonon of sp^2 carbon atoms (D-band) and the breathing mode of K-point phonons of A_{1g} symmetry (G-band), respectively. The intensity ratio of D to G band (I_D/I_G) can be used to evaluate the degree of modification or defects of RGO. In this work, the I_D/I_G value of GO and BSA-RGO composite is 1.27 and 1.52, respectively. The increased I_D/I_G value reveals an increase in the average size of sp^2 domains in RGO compared with GO.
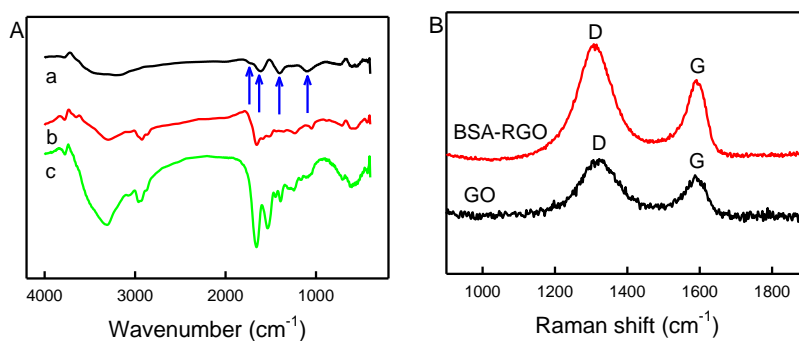
Figure 1. FTIR (A) and Raman (B) spectra of GO and BSA-RGO composite. (Curve a: GO, curve b: BSA-RGO, curve c: BSA)

3.2 Characterization of the modified electrodes

Figure. 2 shows CV curves at different modified electrodes in 0.1 M K_2SO_4 containing 2 mM $K_4Fe(CN)_6$. The bare GCE gave a pair of well-defined redox peaks, with a peak-to-peak separation (ΔE_p) of 69 mV, indicating a reversible electrode process of Fe(CN)$_6^{3-/4-}$ (curve a). After modified with the BSA-RGO composite, a pair of well-defined redox peaks was observed, with a ΔE_p of 129 mV and enhanced capacitive currents (curve b). As for the PtNPs/BSA-RGO /BSA-RGO/GCE, a pair of well-defined redox peaks was also observed, with a ΔE_p of 72 mV and large capacitive currents (curve c). The electron transfer kinetics of Fe(CN)$_6^{3-/4-}$ was also investigated by electrochemical impedance spectroscopy (EIS).
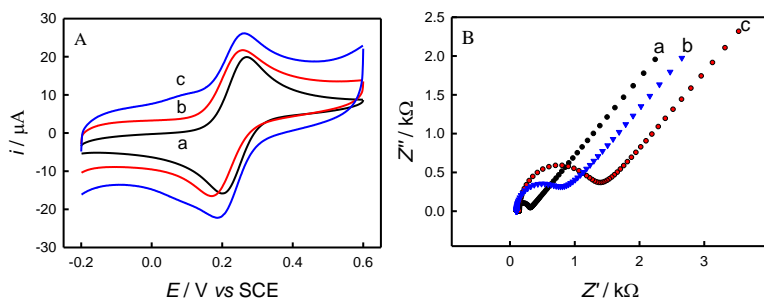
Figure 2. CV (50 mV s^{-1}) and EIS (0.22 V, 100 kHz ~ 0.01 Hz, 5 mV amplitude) curves on bare GCE (curve a), PtNPs/BSA-RGO and BSA-RGO/GCE in 0.1 M K_2SO_4 containing 2 mM $K_4Fe(CN)_6$.

The Nyquist semicircle diameter is equal to the electron transfer resistance (R_{et}), which follows the order bare GCE (194 Ω, curve a) < PtNPs/BSA-RGO (608 Ω, curve g) < BSA-RGO/GCE (1.04 kΩ, curve c). The EIS results have confirmed the conclusions drawn from the above CV experiments.

The morphology of the BSA-RGO/GCE and PtNPs/BSA-RGO /GCE was examined by SEM (Figure. 3). For BSA-RGO, a typical crumpled and wrinkled sheets spread out on the GCE surface (Figure. 3A). After the BSA-RGO/GCE was immersed into a solution containing 1.0 mM $H_2PtCl_6 \cdot 6H_2O$ and 1M HCOOH for 24 h at room temperature, a layer of PtNPs was distributed on BSA-RGO sheets surface (Figure. 3B), this results indicating the Pt/BSA-RGO composite was successfully synthesized by formic acid reduction at room temperature.
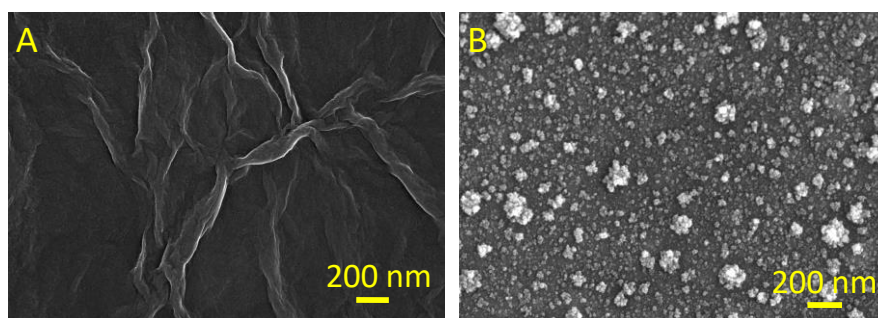

Figure 3. SEM of BSA-RGO/GCE and PtNPs/BSA-RGO/GCE.

3.3 The electro-catalytic effect of PtNPs/BSA-RGO towards glucose in neutral media

The catalytic properties of the PtNPs/BSA-RGO/GCE were investigated using cyclic voltammetry. Figure. 4 shows the CVs of the Pt/BSA-RGO/GCE in 0.1 M PBS (pH=7.4) in the absence (Figure 4a) and presence (Figure 4b) of 20 mM glucose at a potential scan rate of 20 mV s^{-1} respectively. In the blank PBS, the peaks from -0.6 to -0.35 V ascribed to the hydrogen adsorption/desorption peaks, the peaks appeared at 0.25 V forward and 0.02 V in the reverse scan vested to the platinum oxide formation and reduction respectively. Figure. 4b recorded the CVs with 20 mM glucose in the PBS. Comparing to in the blank PBS, the characteristics changed significantly and exhibit a good catalytic activity by the multiple peaks attributed to the adsorption and redox of glucose and its intermediates. Peak I at -0.48 V was ascribed to the electrochemical adsorption of glucose and the dehydrogenation of the anomeric carbon. The peak II appearing associate with the electrosorption of glucose to form gluconic acid, and occurs at the double layer region spanning -0.1 to 0.2 V. At potentials move positive, the Pt surface was covered by the poisoning intermediates, resulting in a current decrease (peak III, at 0.59 V). The decreased current at more positive potential was caused by the formation of thick Pt oxide, which competed for the surface adsorption sites with glucose, and inhibited the direct electrocatalytic oxidation of glucose. In the reverse scan, more and more surface sites would be re-activated with the reduction of platinum oxide at a potential around 0.04 V, resulting in a sharp increase in anodic current with the peak at -0.16 V. After moving to even more negative potential, intermediates of electrocatalytic oxidation of glucose accumulated on PtNPs/BSA-RGO/GCE surface, inducing the anodic current decreased.
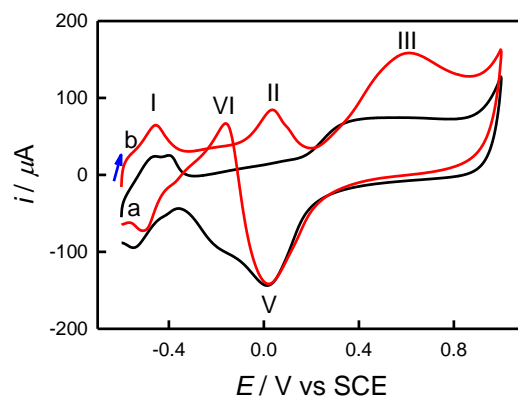
Figure 4. CV curves of PtNPs/BSA-RGO/GCE in 0.1 M PBS (pH 7.4) without (a) and with (b) 20 mM glucose at a scan rate of 20 mV s^{-1}.

The linear sweep voltammetry (LSV) was applied to assess the tolerance of 0.1 M Cl^{-1} on the PtNPs/BSA-RGO/GCE in 0.01 M PBS (pH 7.4) containing 20 mM glucose (Figure. 5). Though the position of the redox peaks for the oxidation of glucose remained unchanged, two obvious differences could be distinguished. Firstly, the peaks height at the potential around 0.02 V was to a certain degree decreased. We think Cl^{-1} may be prior to block active sites on the PtNPs/BSA-RGO/GCE surface, resulting a suppression of glucose adsorption and decreasing the oxidation rate; secondly, the anodic current peaks at a potential around 0.59 V were decreased a little with more symmetrical curve shape in the presence of Cl^{-1}, indicating that Cl^{-1} had seldom effect in the direct electrocatalytic oxidation of glucose. These results proved the PtNPs/BSA-RGO catalyst can be used for glucose electrocatalytic oxidation even in the presence of a high concentration of Cl^{-1}.
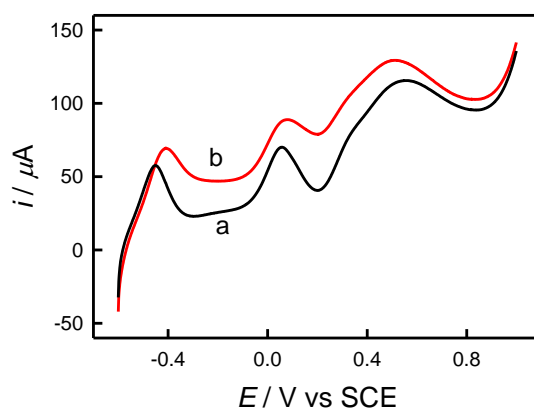

Figure 5. LSV of the fabricated PtNPs/BSA-RGO/GCE in 0.1 M PBS (pH 7.4) containing 20 mM glucose with the absense (a) or presence (b) of 0.1 M KCl at scan rate of 20 mV s^{-1}.

3.4 Amperometric response of PtNPs/BSA-RGO/GCE

Figure. 6 shows the amperometric responses of the PtNPs/BSA-RGO/GCE at the potentials around 0.50 V with difference concentrations glucose added to the stirred solution with optimized experimental conditions. When the glucose was added into the stirred test solution, the current varied steeply to reach a stable value. It was observed that PtNPs/BSA-RGO/GCE respond quickly to the

change of glucose concentration and reach a steady-state current less than 5 s. Its calibration curve displays a linear range from 20 μM to 7.5 mM with a sensitivity of 3.62 mA mM^{-1} cm^{-2} ($r = 0.9972$), and a detection limit of 2.0 Mm ($N/S=3$) which lower than many non-enzymatic electrochemical glucose sensors. The detection limit, linear calibration range and sensitivity for glucose determination at PtNPs/BSA-RGO/GCE were presented in Table 1 comparing to some non-enzymatic glucose sensing methods and materials reported previously. All the characters of the PtNPs/BSA-RGO/GCE were comparable and even better than those reported previously, which meant that the PtNPs/BSA-RGO was promising for analytical applications.
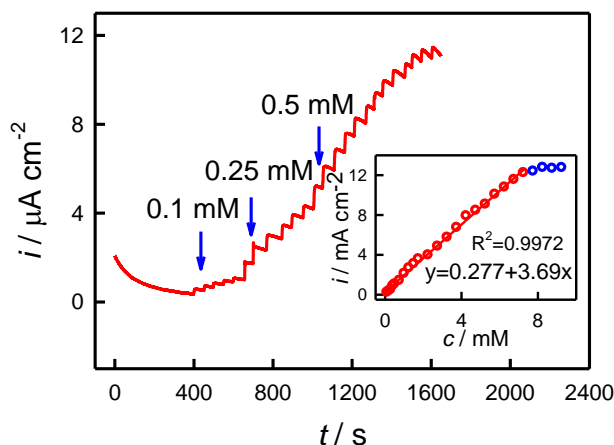

Figure 6. Chronoamperometric responses to successive additions of glucose and the calibration curves (insert) at PtNPs/BSA-RGO/GCE under optimized conditions at the potential of 0.50 V.

Table 1. Comparison of performances of different electrochemical non-enzymatic sensors based on PtNPs-based for determination of glucose in neutral media.

electrode	Sensitivity /μA mM^{-1} cm^{-2}	LOD / μM	Linear rang /mM	Potential / V *vs* SCE	Reference
PtNFs-GO/GCE	1.26	2	0.002~10.3	0.47	[27]
PtNCs-RGO/GCE	1.21	30	1~25	0.05	[21]
Pd$_1$Pt$_3$-RGO/GCE	-	5	1~23	0.1	[41]
Pt/MWCNT/GCE	1.10	-	2~20	0.55	[42]
PtNEGHNs/GCE	10.8	-	1~16	0	[43]
PtNi-eRGO/GCE	20.42		~35	-0.35	[44]
PtNPs/BSA-RGO/GCE	3.69	2	0.02~7.5	0.50	This work

PtNFs: platinum nanflowers; PtNEGHNs: Pt nanoparticle ensemble-on-graphene hybrid nanosheet.

3.5 Stability, reproducibility and selectivity of PtNPs/BSA-RGO/GCE

The stability of the PtNPs/BSA-RGO/GCE was investigated by comparing the changes of current response, it was found that the biosensor showed only a decay of 13% of its initial response

current after the two weeks of storage. The repeatability of the biosensor was also investigated by the amperometric responses of 8 successive measurements. The relative standard deviation (RSD) value was found to be 4.6%. These results suggesting that there was little inhibition effect of glucose, and the PtNPs/BSA-RGO suitable for construct sensitive, stable and reproducible non-enzymatic glucose sensors in neutral media.

In non-enzymatic glucose detection, the interfering electrochemical signals is always caused by some coexisting organic substances such as ascorbic (AA) and (UA) in real samples. The effects of interfering species of AA and UA on PtNPs/BSA-RGO/GCE were examined just as shown in Figure.7. The amperometric response of the biosensor to consecutive injection of 1 mM glucose and interfering species including 0.2 mM AA and UA. The PtNPs/BSA-RGO/GCE exhibited high sensitivity to glucose oxidation and depressed responses towards these interceptors.
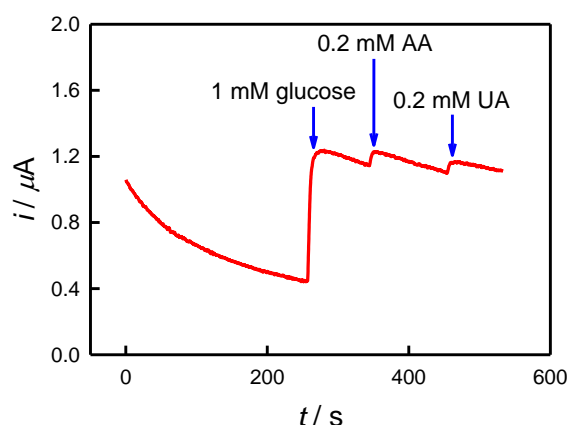

Figure 7. The response of PtNPs/BSA-RGO/GCE of the additions of 0.2 mM ascorbic acid (AA) and uric acid (UA) at 0.50 V in PBS to addition of 1.0 mM glucose.

3.6 The real samples analysis of the PtNPs/BSA-RGO/GCE

In order to evaluate the applicability of the PtNPs/BSA-RGO/GCE, it was used for the determination of glucose in glucose injection samples. Four samples with the known glucose concentrations were sampled and certain amounts of glucose were added. The recoveries of the detection of glucose was in the range of 99.3% to 101.3%, indicating that the prepared sensor has high accuracy in measuring the real sample.

Table 2. Recovery test of glucose at PtNPs/BSA-RGO/GCE

Sample	Glucose concentration (mM)	Added amounts *(mM)	Measured (mM)	Recovery (%)
1	0	2.0	2.01	100.5
2	0	2.0	2.05	102.5
3	1	4.0	4.97	99.3
4	1	4.0	5.07	101.3

* Glucose injection samples were obtained from a local hospital and diluted with PBS (pH 7.4) containing 0.1 M NaCl.

4. CONCLUSIONS

A novel non-enzymatic glucose sensor based on a PtNPs/BSA-RGO nanostructure was developed. The BSA-RGO was synthesized using a hydrothermal synthesis method with BSA acted as the reductant and stabilizing reagent, and the PtNPs were reduced onto the BSA-RGO/GCE with the formic acid as the reduction at room temperature. Electrochemical observation showed the PtNPs/BSA-RGO/GCE had high electrocatalytic activity for glucose oxidation in neutral solution, the linear range, sensitivity, reproducibility and selectivity were acceptable, which can be found extensive application in non-enzymatic glucose sensors.

References

1. S.J. Updike, M.C. Shults, B.J. Gilligan, R.K. Rhodes, *Diabetes Care*, 23 (2000) 208.
2. E. Dolgin, *Nature*, 485 (2012) S6.
3. C. Chen, Q. Xie, D. Yang, H. Xiao, Y. Fu, Y. Tan, S. Yao, *RSC Adv.*, 3 (2013) 4473.
4. X.H. Niu, L.B. Shi, H.L. Zhao, M.B. Lan, *Anal. Methods*, 8 (2016) 1755.
5. M.S. Steiner, A. Duerkop, O.S. Wolfbeis, *Chem. Soc. Rev.*, 40 (2011) 4805.
6. X. Wu, L.R. Lin, Y.J. Huang, Z. Li, Y.B. Jiang, *Chem. Commun.*, 48 (2012) 4362.
7. T. Saxl, F. Khan, M. Ferla, D. Birch, J. Pickup, *Analyst,* 136 (2011) 968.
8. R. Weiss, Y. Yegorchikov, A. Shusterman, I. Raz, *Diabetes Technol.*, 9 (2007) 68.
9. L. Fang, B. Liu, L. Liu, Y. Li, K. Huang, Q. Zhang, *Sens. Actuator B: Chem.*, 222 (2016) 1096.
10. Y. Song, Y. Luo, C. Zhu, H. Li, D. Du, Y. Lin, *Biosens. Bioelectron.*, 76 (2016) 195.
11. J. Wang, *Chem. Rev.*, 108 (2008) 814.
12. R. Wilson, A.P.F. Turner, *Biosens. Bioelectron.*, 7 (1992) 165.
13. R. Hang, Y. Liu, A. Gao, L. Bai, X. Huang, X. Zhang, N. Lin, B. Tang, P.K. Chu, *Mat. Sci. Eng.: C*, 51 (2015) 37.
14. J. Dong, T. Tian, L. Ren, Y. Zhang, J. Xu, X. Cheng, *Colloids Surf B: Biointerfaces*, 125 (2015) 206.
15. M. Baghayeri, A. Amiri, S. Farhadi, *Sens. Actuator B: Chem.*, 225 (2016) 354.
16. S. Fu, G. Fan, L. Yang, F. Li, *Electrochim. Acta*, 152 (2015) 146.
17. L. Ruiyi, Z. Juanjuan, W. Zhouping, L. Zaijun, L. Junkang, G. Zhiguo, W. Guangli, *Sens. Actuator B: Chem.*, 208 (2015) 421.
18. Y. Luo, F.Y. Kong, C. Li, J.J. Shi, W.X. Lv, W. Wang, *Sens. Actuator B: Chem.*, 234 (2016) 625.
19. F. Xie, Z. Huang, C. Chen, Q. Xie, Y. Huang, C. Qin, Y. Liu, Z. Su, S. Yao, *Electrochem. Commun.,* 18 (2012) 108.
20. R. Krishna, D.M. Fernandes, A. Marinoiu, J. Ventura, C. Freire, E. Titus, *Int. J. Hydrogen Energ.,* 42(2017)23639.
21. G. Chang, H. Shu, Q. Huang, M. Oyama, K. Ji, X. Liu, Y. He, *Electrochim. Acta*, 157 (2015) 149.
22. L.T. Hoa, K.G. Sun, S.H. Hur, *Sens. Actuator B: Chem.*, 210 (2015) 618.
23. Y. Song, C. Zhu, H. Li, D. Du, Y. Lin, *RSC Adv.*, 5 (2015) 82617.
24. H. Zhu, L. Li, W. Zhou, Z. Shao, X. Chen, *J. Mater. Chem. B*, 4 (2016)7333.
25. Y. Zhang, Y. Liu, L. Su, Z. Zhang, D. Huo, C. Hou, Y. Lei, *Sens. Actuator B: Chem.*, 191 (2014) 86.
26. C. Guo, H. Li, X. Zhang, H. Huo, C. Xu, *Sens. Actuator B: Chem.*, 206 (2015) 407.
27. G.h. Wu, X.h. Song, Y.F. Wu, X.m. Chen, F. Luo, X. Chen, *Talanta*, 105 (2013) 379.
28. X. Niu, M. Lan, C. Chen, H. Zhao, *Talanta,* 99 (2012) 1062.
29. S.H. Kim, J.B. Choi, Q.N. Nguyen, J.M. Lee, S. Park, T.D. Chung, J.Y. Byun, *Phys. Chem. Chem. Phys.*, 15 (2013) 5782.

30. Q. Li, W. Luo, L. Su, J. Chen, K.C. Chou, X. Hou, *RSC Adv*., 6 (2016) 92748.
31. C.C. Mayorga-Martinez, M. Guix, R.E. Madrid, A. Merkoci, *Chem. Commun*., 48 (2012) 1686.
32. Y. Zhang, W. Lei, Q. Wu, X. Xia, Q. Hao, *Microchim. Acta*,184 (2017)3103.
33. S. Park, R.S. Ruoff, *Nat Nano*, 4 (2009) 217.
34. Y. Matsumoto, M. Koinuma, S.Y. Kim, Y. Watanabe, T. Taniguchi, K. Hatakeyama, H. Tateishi, S. Ida, *ACS Appl. Mater. Interf*., 2 (2010) 3461.
35. P.V. Kamat, *J. Phys. Chem. Lett*., 1(2010) 520.
36. Y. Liu, Y. Dong, C.X. Guo, Z. Cui, L. Zheng, C.M. Li, *Electroanalysis,* 24 (2012) 2348.
37. H. Shu, G. Chang, J. Su, L. Cao, Q. Huang, Y. Zhang, T. Xia, Y. He, *Sens. Actuator B: Chem*., 220 (2015) 331.
38. H.D. Jang, S.K. Kim, H. Chang, J.W. Choi, J. Huang, *Mater. Lett.,* 106 (2013)277.
39. J. Liu, S. Fu, B. Yuan, Y. Li, Z. Deng, *J. Am. Chem. Soc*., 132 (2010) 7279.
40. M. Li, X. Bo, Z. Mu, Y. Zhang, L. Guo, *Sens. Actuator B: Chem*., 192 (2014) 261.
41. H. Zhang, X. Xu, Y. Yin, P. Wu, C. Cai, *Sens. Actuator B: Chem*., 690 (2013) 19.
42. D. Rathod, C. Dickinson, D. Egan, E. Dempsey, *Sens. Actuator B: Chem*., 143 (2010) 547.
43. S. Guo, D. Wen, Y. Zhai, S. Dong, E. Wang, *ACS Nano*, 4 (2010) 3959.
44. H. Gao, F. Xiao, C.B. Ching, H. Duan, *ACS Appl. Mater. Interf*., 3 (2011) 3049